

# Theoretical investigation of the interaction of CH<sub>4</sub> with Al<sub>2</sub> and Al<sub>3</sub> neutral and charged clusters

E.I. Alexandrou,<sup>1</sup> A. Groß,<sup>2</sup> and N.C. Bacalis<sup>1</sup>

<sup>1</sup>*Theoretical and Physical Chemistry Institute, National Hellenic Research Foundation, Athens 11635, Greece*

<sup>2</sup>*Institute for Theoretical Chemistry, Ulm University, D-89069 Ulm, Germany*

(Dated: March 11, 2010)

We have studied the interaction of CH<sub>4</sub> with Al<sub>2</sub> and Al<sub>3</sub> neutral and charged clusters in the two lowest lying spin states using density functional theory. These calculations, via extended search, are used to determine the stable positions of H and CH<sub>3</sub> near the cluster, and the transition state to break the H - CH<sub>3</sub> bond. In all cases, stable methyl-aluminum-hydrides are possible. The H desorption is studied by means of vibration analysis and application of transition state theory. A common observed trend is that, in breaking the H-CH<sub>3</sub> bond, the interacting H atom is attached to the “surface” of the clusters attracting some negative charge of  $\approx 0.2$  e. The charge transfer is illustrated using the corresponding orbitals near the transition state in conjunction with the computed Mulliken population analysis. Thermal vibrations, generally, do not enhance the reaction. In all exothermic cases, the binding energy toward CH<sub>3</sub> + HAl<sub>n</sub><sup>charge</sup> increases with increasing charge of the original Al<sub>n</sub><sup>(q=-1,0,1)</sup> cluster. Although Al lacks occupied d-orbitals, the small Al clusters reduce the (free methane) CH<sub>3</sub>-H dissociation barrier except for Al<sub>3</sub><sup>(q=-1,0)</sup>. The relevant reactions in desorption require  $\sim 400$ -700 °C.

## I. INTRODUCTION

In the last decades, cluster research has been one very active scientific research field. Through covering the range from noble gas systems held together by the weak dispersion force over metallic clusters to covalent bound species, the cluster systems can all be seen as representing a link between the gaseous and the condensed phase. Still, clusters often possess unique properties different from those of both the extended bulk and the atomic states. Consequently, the size evolution of various cluster properties, such as equilibrium geometries, stability, bonding nature, ionization potential, etc. [1, 2] and their interaction with other species represents an interesting and challenging problem. Further, nanosized metal clusters and their reactivity are highly relevant in understanding the basal processes behind heterogeneous catalysis, corrosion and passivation [3, 4] since catalysts and device materials often exhibit nanostructured surfaces containing small adsorbed clusters.

During the past decades the C-H and C-C bond activations of small alkanes and olefins in the gas phase by transition-metal ions have received a great deal of attention both experimentally and theoretically for the potential economic and environmental significance and considerable fundamental interest [5].

Apart from the alkali-metal clusters, the aluminum clusters are among the most thoroughly investigated systems, both theoretically and experimentally [1, 2, 6–9]. Aluminum is a good free electron metal in the bulk state, and seems ideal for an intense study because of the ease with which it is ionized. Moreover, its cluster anions are readily produced because they have a relatively high electron affinity, but it is also possible to form positively charged aluminum clusters [1, 6–8]. Furthermore, its relatively simple valence electronic structure makes Al clus-

ters amenable to quantum chemical calculations [7].

In spite of the free-electron nature of bulk aluminum, several experimental and theoretical studies indicate that the small aluminum clusters do not display the well-known “magic” behavior [1, 9] for the stability of the clusters as a function of the number of Al atoms. Instead, rather an odd-even pattern in the number of electrons has been observed, as far as their stability [1, 9] and the reactivity with oxygen [10] are concerned. In contrast to transition metal clusters, Al clusters have a rather small spin-orbit coupling. This makes spin selection rules and spin conservation rather important for Al clusters [11]. In fact, it has been suggested that the dissociation dynamics of Al clusters is controlled by spin selection rules [1]. Spin conservation is also important for the interaction of molecules with Al [12]. It has been shown that spin selection rules could play an important role in understanding the dissociation dynamics of O<sub>2</sub>/Al(111) [13–16] which exhibits a surprisingly low probability for O<sub>2</sub> impinging at low kinetic energies on Al(111) [17]. And indeed, the importance of spin-selection rules for the interaction of oxygen with small anionic clusters formed of  $\sim 10 - 20$  Al atoms was recently confirmed experimentally [18].

Whereas the interaction of oxygen with Al clusters has been studied intensively, relative few studies have been devoted to the interaction of hydrocarbons with Al clusters. Hydrocarbons, especially methane, are urgently important for energy conversion and storage due to their high hydrogen concentration. A prospective process for the utilization of natural gas resource is the dehydrogenation-aromatization of methane in the absence of O<sub>2</sub> where the yielded higher hydrocarbons can be easily separated from the reaction moiety. The byproduct molecular hydrogen is of great interest to industry since it is a clean energy source. Although the process is thermodynamically not favorable at low temperatures, it

has become one of the frontiers in the field of methane activation chemistry. Compared to the oxidative coupling of methane, which is another developing process for the utilization of methane, dehydrogenation is less complicated [19]. It was claimed that Al clusters are inactive with methane ( $\text{CH}_4$ ) [10]. Usually, the C-H bond activation of alkanes is catalyzed by transition metals [4, 20–23] which suggests that the involvement of d-electrons is necessary for the C-H bond breaking. However, the extent to which the geometric local environment is responsible for the activation, compared to the d-electron interaction, is not clear yet. Furthermore, spin conservation effects are known to be important in methane dissociation [11], however, their particular role in the interaction of methane with small Al clusters is still unclear. It should also be noted that methyl-aluminum hydrides which are created in the dissociation of methane on the Al clusters are important in the chemical vapor deposition of Al [24, 25].

Hence we decided to study the interaction of methane with small clusters of aluminum atoms using quantum chemical calculations. We consider small clusters of  $\text{Al}_2$  and  $\text{Al}_3$  with charge 0, 1, and -1 e, interacting with  $\text{CH}_4$  in the two lowest states of the total spin. Thus a varying number of electrons and consequently different spin states of the Al clusters are considered. Indeed, we find a strong correlation between the reactivity of methane with the Al clusters and the spin multiplicity as well as the charge of the clusters.

## II. COMPUTATIONAL DETAILS

Our calculations were performed within density functional theory (DFT) [26–28] using the Gaussian03 package [29] employing the 6-31G(d,p) basis [30] and the B3LYP exchange and correlation functional [31]. In order to choose the basis set and the exchange and correlation functional we computed the energy along a fictitious “reaction path” of dissociation of the methyl-aluminum-hydride  $\text{CH}_3\text{-Al}_2\text{-H}$  toward  $\text{CH}_4 + \text{Al}_2$  (cf. Fig. 1), using the basis sets 3-21G, 6-31G, 6-311G [32], both bare and augmented by polarization functions, with the (i) B3LYP and (ii) PBE exchange and correlation functionals [33]: After finding a stable geometric structure of  $\text{CH}_3\text{-Al}_2\text{-H}$  by one of these choices (6-31G/B3LYP), in all these tests we considered seven possible configurations of  $\text{CH}_3$  and H (C-H always parallel to the equilibrium direction) labeled in the figure from “0” (H very close to C) to “6” (beyond the equilibrium), as seen in the inset of the figure, where the hydride equilibrium configuration is labeled by “5” whereas the configuration with the normal methane C-H bond length is labeled by “1”. Each configuration is obtained by displacing the atoms of C and H along straight lines passing through their “1” and “5” positions. The x-axis of the figure is the C-X line in the inset, typically perpendicular to the C-H direction of each configuration.

Although the absolute values of the total energy differ in the various schemes, in the figure we shifted all

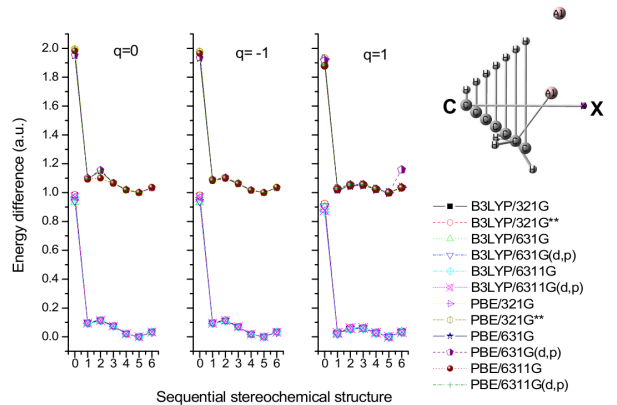


FIG. 1: Energies of a sequence of geometrical structures computed with 3-21G, 6-31G, and 6-311G basis functions, both bare and augmented with polarization functions, and with B3LYP and PBE exchange and correlation potentials. The horizontal axis labels from 0 to 6 the consecutive structures depicted in the inset, in moving along the CX line. The H atoms of  $\text{CH}_3$  are displayed in only one structure.

graphs to a common value at the equilibrium structure “5”, namely to 0.1 a.u. for the B3LYP functional and to 1.1 a.u. for the PBE functional. As seen from the figure the differences are negligible compared to the reaction energies. However, in some cases PBE erroneously converges to higher local energy minima probably corresponding to non-adiabatic extrapolations beyond avoided crossings, as observed in previous DFT calculations addressing the interaction of molecules with Al clusters [12]. Because these avoided crossings are *a priori* unknown, the reliability of the computed values can hardly be assessed. Thus we choose the 6-31G basis for our study which provides an acceptable compromise between accuracy and numerical efficiency, augmented by polarization functions. As far as the relevance of our calculations for the understanding of the reactivity of extended substrates is concerned, please recall the generally known observation that cluster calculations yield qualitative trends rather than quantitative results when they are applied to surface problems [34–36].

The Al clusters exhibit a multitude of different spin configurations. The determination of the correct energy minimum states can be quite problematic in such a case [12]. Furthermore, with respect to the observation that the B3LYP functional does not always describe the dissociation limit correctly at all spin states, we considered the two lowest spin states of the whole system  $\text{Al}_n\text{-CH}_4$ , which are singlet-triplet or doublet-quartet depending on the total charge, in order to check whether during the approach of the fragments spin flipping needs to be taken into account.

Within this work, we focus on the configuration and

the energy of the transition state for the reaction



with  $n = 2, 3$  and the  $\text{Al}_n^q$  cluster in three different charge states  $q = -1, 0, +1e$ . We will refer to the barrier for the forward barrier as the ‘‘adsorption barrier’’ (in analogy to the reaction with a solid Al surface) which corresponds to the dissociative attachment of methane to the Al cluster involving the breaking of a  $\text{CH}_3\text{-H}$  bond. The barrier for the backward reaction we will denote as the ‘‘desorption barrier’’ which corresponds to the recombinative detachment of methane from the Al cluster with the  $\text{H-Al}_n$  and  $\text{CH}_3\text{-Al}_n$  being broken.

Finding the transition state for these reactions is not trivial. Therefore we first located an approximate transition state by mapping out certain two-dimensional cuts through the high-dimensional potential energy surface and used this configuration as the starting point for an automatic search using the Transition State Quasi Newton (TSQN) algorithm [37]. In detail, we adopted the following strategy:

1) By geometry optimization we located the most stable position of a hydrogen atom in the vicinity of the cluster.

2) Similarly we located the most stable position of a  $\text{CH}_3$  fragment in the vicinity of the previously determined  $\text{Al}_n\text{H}$ .

3) We relaxed the last positions to form a  $\text{CH}_3\text{-Al}_n\text{H}$  complex, in which we call the axis containing C (of  $\text{CH}_3$ ) and H (of  $\text{Al}_n$ ) the ‘‘stability axis’’.

4) We considered several consecutive planes passing through the ‘‘stability axis’’, separated by  $30^\circ$  between each other, which we label by the degree of rotation as planes of  $30^\circ, 60^\circ, 90^\circ, 120^\circ, 150^\circ,$  and  $180^\circ = 0^\circ$ .

5) On each plane we considered a grid of points intersecting the stability axis in a parallel (‘‘x’’) and a perpendicular (‘‘y’’) fashion. Keeping the  $\text{Al}_n$  clusters constant at each plane, we moved, on the ‘‘y’’ axis, the  $\text{CH}_3$  perpendicularly to the stability axis (with  $\text{H}_3$  relaxed) and for each  $\text{CH}_3$  position we moved the 4th H atom parallelly to the stability ‘‘x’’ axis. The grid points were separated by  $0.5 \text{ \AA}$ .

6) By computing the total energy at each of the above positions we obtained a contour diagram of equal energy values for each plane.

7) On each plane we located the lowest lying saddle point.

8) We plotted the energy as well as the x- and y-coordinates of the above saddle points versus the angle of the plane’s rotation, and, by interpolation, we determined the angle of the lowest lying saddle point among all angles, which we call the ‘‘TS’’ angle.

9) By interpolating the x- and y-coordinates of the saddle points at the TS angle we obtained an estimate of the transition state for the  $\text{H-CH}_3$  bond breaking (identified by x,y, and energy).

10) Using this as an initial configuration for the TSQN algorithm [37], we calculated precisely the true transition

state by relaxing all coordinates.

### III. INTERACTION OF METHANE WITH $\text{Al}_2$ AND $\text{Al}_3$ CLUSTERS

#### A. $\text{Al}_2 + \text{CH}_4$

The  $\text{Al}_2$  dimer has already been well-studied [39–41]. Its ground-state is known to be  ${}^3\Pi_u$  ( $1\pi_u 2\sigma_g$ ) with its minimum at an Al-Al distance of  $2.76 \text{ \AA}$ , slightly lower in energy than the  ${}^3\Sigma_g^-$  ( $1\pi_u^2$ ) state with its minimum at an Al-Al distance of  $2.51 \text{ \AA}$ . The reason for the two almost degenerate minima is a transitional crossing of the  $1\pi_u$  with the  $2\sigma_g$  valence Kohn-Sham orbitals at Al-Al distance about  $2.6 \text{ \AA}$  (see also Ref. [38]). The two lowest lying spin states at equilibrium of all considered structures are given in Table I.

The equilibrium structure of  $\text{HAl}_2$  is given in Fig. 2(a1) (doublet) and 2(a2) (quartet), with energies  $E = -485.3966 E_h$  and  $-485.3587 E_h$  respectively; therefore, the most stable structure is the doublet,  $3.04 \text{ eV}$  lower than the separated  $\text{Al}_2$  and H. By inserting  $\text{CH}_3$ , the most stable structure between singlet [Fig. 3(a1)] and triplet [Fig. 3(a2)] is the singlet,  $E = -525.333 E_h$ ,  $0.43 \text{ eV}$  ( $10 \text{ kcal/mol}$ ) lower than the separated  $\text{Al}_2$  and  $\text{CH}_4$ , where  $\text{Al}(2)\text{-Al}(1) = 2.67 \text{ \AA}$ ,  $\text{C}(3)\text{-Al}(2) = 1.99 \text{ \AA}$ ,  $\text{C}(3)\text{-Al}(2)\text{-Al}(1) = 150^\circ$ ,  $\text{H}(7)\text{-Al}(2) = 1.87 \text{ \AA}$ ,  $\text{H}(7)\text{-Al}(2)\text{-Al}(1) = 45^\circ$ , and dihedral angle  $\text{H}(7)\text{-Al}(2)\text{-Al}(1)\text{-Al}(2)\text{-Al}(1)\text{-C}(3) = 0^\circ$ . The contour energy diagram in planes passing through the common x-axis of C-H(7), consecutively rotated by  $30^\circ$  from each other, are shown in Fig.

Species	Ground state ( $E_h$ )	Excited state ( $E_h$ )
$\text{CH}_3$	-39.8269 (2)	-39.3851 (4)
$\text{CH}_4$	-40.5169 (1)	-40.0693 (3)
$\text{Al}_2$	-484.7850 (3)	-484.7706 (1)
$\text{Al}_2 \text{ H}$	-485.3966 (2)	-485.3587 (4)
$\text{Al}_2 \text{ HCH}_3$	-525.3333 (1)	-525.3169 (3)
$\text{Al}_2^+$	-484.5697 (2)	-484.4651 (4)
$\text{Al}_2 \text{ H}^+$	-485.1851 (1)	-485.0961 (3)
$\text{Al}_2^+ \text{ HCH}_3$	-525.0911 (2)	-525.0035 (4)
$\text{Al}_2^-$	-484.8297 (4)	-484.8052 (2)
$\text{Al}_2 \text{ H}^-$	-485.4402 (3)	-485.4210 (1)
$\text{Al}_2^- \text{ HCH}_3$	-525.3689 (2)	-525.3395 (4)
$\text{Al}_3$	-727.2227 (2)	-727.2137 (4)
$\text{Al}_3 \text{ H}$	-727.8319 (1)	-727.8269 (3)
$\text{Al}_3 \text{ HCH}_3$	-767.7738 (2)	-767.7462 (4)
$\text{Al}_3^+$	-726.9895 (3)	-726.9753 (1)
$\text{Al}_3 \text{ H}^+$	-727.8319 (2)	-727.5511 (4)
$\text{Al}_3^- \text{ HCH}_3$	-767.5507 (1)	-767.5242 (3)
$\text{Al}_3^-$	-727.2839 (1)	-727.2679 (3)
$\text{Al}_3 \text{ H}^-$	-727.8789 (2)	-727.8702 (4)
$\text{Al}_3^- \text{ HCH}_3$	-767.8128 (1)	-767.8082 (3)

TABLE I: The energies of the two lowest lying states at equilibrium of all species considered in this work in atomic units (Hartree). The spin multiplicity is shown in parenthesis.

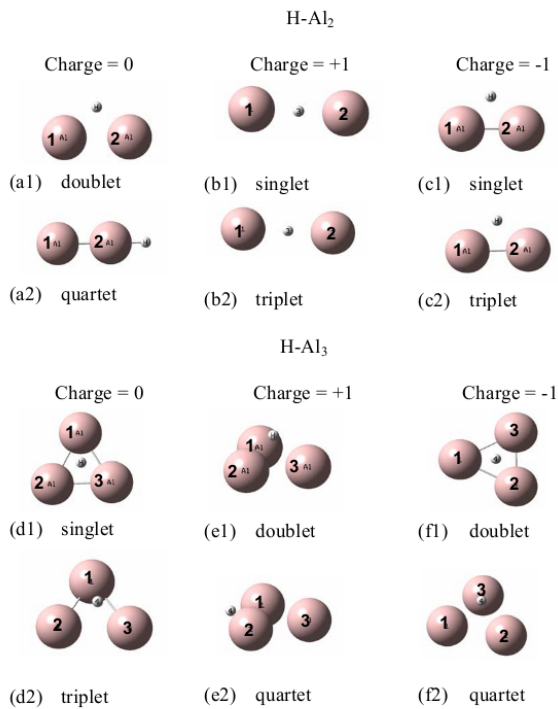


FIG. 2: The equilibrium structure of  $\text{HAl}_n^q$  at the two lowest lying spin multiplicities. Charge  $q = 0, 1, -1$ ,  $n = 2, 3$ . The exact atomic coordinates are mentioned in the text.

4. In these diagrams the y-axis denotes the height of the (relaxed)  $\text{CH}_3$  from its original position on the x- (“stability”) axis which represents the C-H(7) distance. In each diagram there are saddle points whose energies, y-, and x-values are plotted in Fig. 5 (a1,a2,a3) versus the angular position of the diagram’s plane. As seen in Fig. 4, there are two potential wells: One at large separations of  $\text{CH}_3$  from the Al cluster, where the transmitted H atom stays stably as  $\text{CH}_4$  at x-bond length 1.07 Å and  $E = -525.295 E_h$  (there is an equivalent potential well at negative y values). In the other potential well the transmitted H atom stays stably between the two Al atoms ( $y = 0$  Å,  $x = 3$  Å) with  $E = -525.333 E_h$ . Between the two potential wells there is a saddle point for each plane examined, the lowest of which is used as a starting geometry to locate the true transition state (potential barrier = 2.04 eV).

Consider, for example, the contour energy diagram along the plane labeled “60” in Fig. 4 (rotated by 30° from the C-Al-Al-H(7) plane). The upper part ( $y > 0$ ) shows the energy of the system as  $\text{CH}_3$  drops down to its equilibrium position, while H(7) approaches  $\text{CH}_3$  parallel to the x- (“stability”) axis. We observe that at large y-values, far from  $\text{Al}_2$ , H(7) stays stably at  $x=1.07$  Å, the bond length in  $\text{CH}_4$ , so that  $\text{CH}_4$  does still not interact with  $\text{Al}_2$ . At smaller y-values ( $y > 0$ ), H(7) prefers to stay away from  $\text{CH}_3$  just above the two Al atoms. Yet, there is also another, not so stable position of H(7) on the

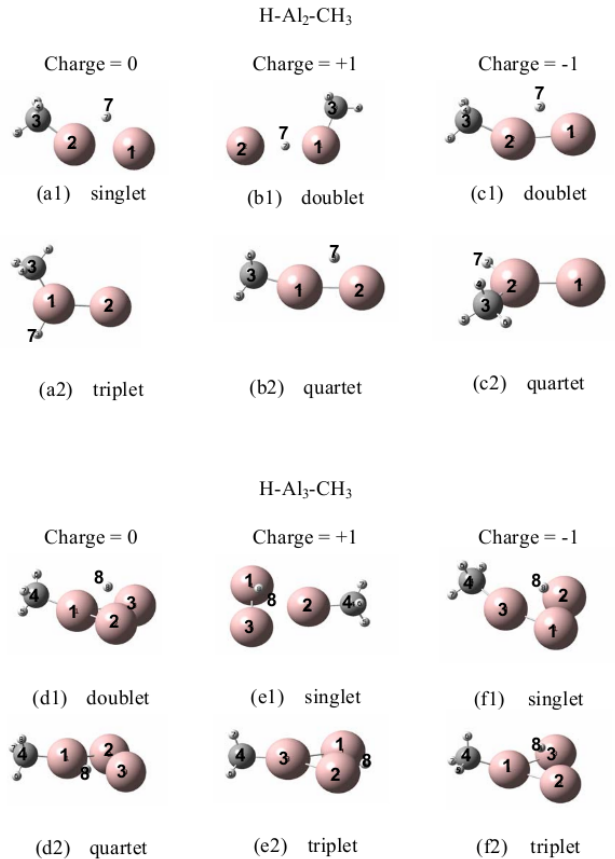


FIG. 3: The most stable structure of  $\text{CH}_3\text{-HAl}_n^q$  at the two lowest lying spin multiplicities. Charge  $q = 0, 1, -1$ ,  $n = 2, 3$ . The exact atomic coordinates are mentioned in the text.

other side of  $\text{Al}_2$ , opposite to  $\text{CH}_3$  ( $x=5.5$  Å). Therefore, we consider the first one as more stable. On this diagram there is a saddle point ( $x=1.7$ ,  $y=2.5$ ), which H(7) has to pass in going from  $\text{CH}_4 + \text{Al}_2$  to  $\text{CH}_3 + \text{Al}_2\text{H}$  (on this plane). This point is not in our grid, so we compute its energy individually. Similar observations are made for the lower part ( $y < 0$ ), which in the analysis we consider as “upper” part of 60+180°. The energies of all these saddle points are plotted against the angle of the plane in [Fig. 5(a1)] while their positions y and x are plotted in the (a2) and (a3) parts of the same figure. By interpolating the energy between the angles we see that the lowest saddle point occurs at an angle of 30° with  $x = 1.80$  Å,  $y = 1.92$  Å,  $E = -525.2549 E_h$ . Starting from this (see Fig. 6(a1)) and by relaxing all coordinates, we obtain using the TSQN algorithm [37] the lowest lying transition state (singlet) shown in Fig. 6(a2) with  $E = -525.2582 E_h$ , where  $\text{Al}(2)\text{-Al}(1) = 2.91$  Å,  $\text{C}(3)\text{-Al}(2) = 2.34$  Å,  $\text{C}(3)\text{-Al}(2)\text{-Al}(1) = 90^\circ$ ,  $\text{H}(7)\text{-C}(3) = 1.48$  Å,  $\text{H}(7)\text{-C}(3)\text{-Al}(2) = 49^\circ$ , dihedral angle  $\text{H}(7)\text{-C}(3)\text{-Al}(2)/\text{C}(3)\text{-Al}(2)\text{-Al}(1) = 0^\circ$ . Thus, in our approximation, the dissociation barrier for the H- $\text{CH}_3$  bond breaking (adsorption barrier) is 0.972 eV and the dissociation barrier for the bond H-

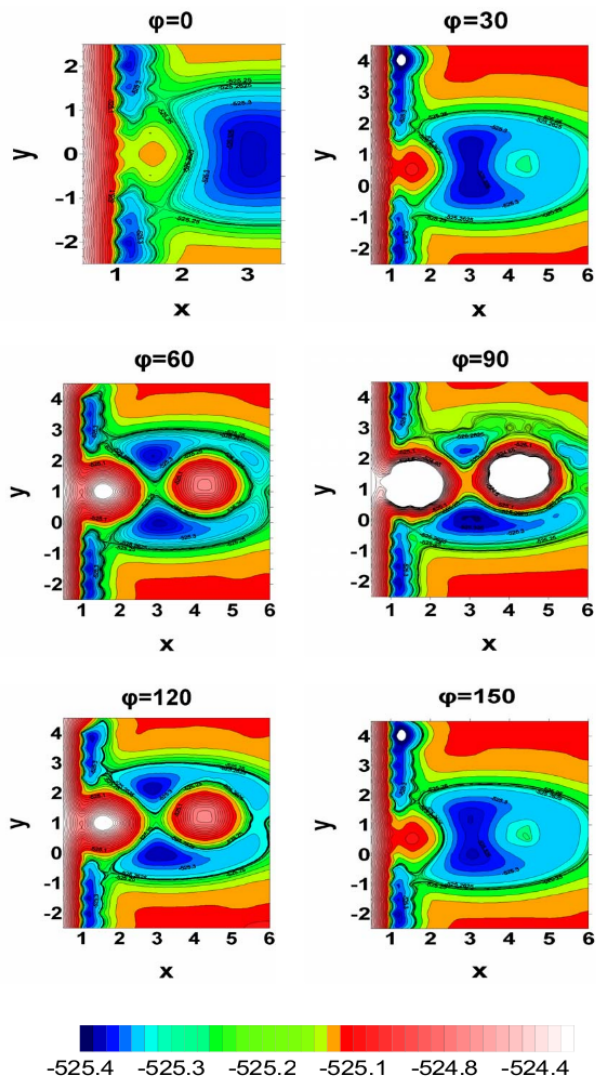


FIG. 4: Contour energy diagrams (in  $E_h$ ) for  $\text{Al}_2$  in planes passing through the common x-axis of C-H(7) consecutively separated by  $30^\circ$  from each other, in which H(7) is the transmitted H. We have six contour energy diagrams for every angle  $\phi$  in which  $y$  ( $y$ -axis) represents the  $\text{CH}_3$  displacement from equilibrium (in  $\text{\AA}$ ) and  $x$  ( $x$ -axis) represents the  $\text{CH}_3$ -H distance (in  $\text{\AA}$ ). Note that  $-|y|$  at  $\phi$  means  $|y|$  at  $\phi + \pi$ . (For  $\text{Al}_3$ , H(7) is replaced by H(8)). The white color means high lying or unconverged results.

$\text{Al}_2\text{CH}_3$  (desorption barrier) is 2.04 eV. We make similar estimates for all clusters, allowing us to draw general conclusions later on.

The corresponding Mulliken atomic charges for the “reactants”  $\text{CH}_4 + \text{Al}_2$ , “product”  $\text{CH}_3 + \text{HAL}_2$ , and the transition state are given in Table II. We observe that in the isolated systems  $\text{Al}_2$  is neutral, as well as  $\text{CH}_4$ , in which C attracts some electronic charge of 0.5 e. In the  $\text{CH}_3$ - $\text{HAL}_2$  complex, mainly H(7) and C (to some lesser extent) attract some electronic charge from the two Al

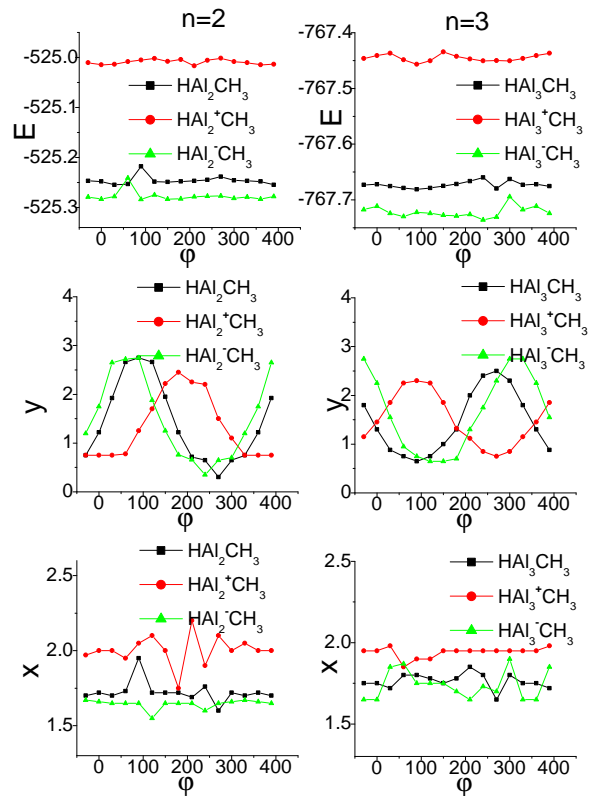


FIG. 5: The saddle points of each diagram of Fig. 4 for  $\text{Al}_2 + \text{CH}_4$  [also for all  $\text{Al}_n^q + \text{CH}_4$ ,  $q = 0, 1, -1$ ,  $n = 2, 3$ ], versus the rotation angle  $\phi$  of the corresponding planes.  $E$  represents the energy (in  $E_h$ ),  $y$  represents the  $\text{CH}_3$  displacement from equilibrium (in  $\text{\AA}$ ), and  $x$  represents the  $\text{CH}_3$ -H distance (in  $\text{\AA}$ ) of the transmitted H. Note that  $(x, -|y|, E)$  at  $\phi$  of Fig. 4 means  $(x, |y|, E)$  at  $\phi + 180^\circ$  in this figure.

atoms, while the three outer H atoms remain unaffected. In the transition state, C attracts almost one electron mainly from the three H atoms while H(7) is neutral and the two Al atoms are slightly positive. Thus, for the transition process, a total electronic charge is attracted from  $\text{CH}_4$  toward the cluster, eventually distributed around H(7). We shall see that a similar charge movement and redistribution occurs in all cases.

## B. $\text{Al}_2^+ + \text{CH}_4$

The ground state of  $\text{Al}_2^+$  has  $^2\Sigma_g^+$  symmetry, and its bond length is 3.34  $\text{\AA}$ , in agreement with Sun *et al.* [9]. The two lowest lying spin states at equilibrium are given in Table I. The equilibrium structure of  $\text{HAL}_2^+$  is given in Fig. 2(b1) (singlet) and Fig. 2(b2) (triplet), where H is located between the two Al atoms, in the middle in the singlet state ( $\text{H-Al} = 1.92 \text{\AA}$ ) and closer to one of the Al atoms in the triplet state ( $\text{H-Al}(1) = 1.68$

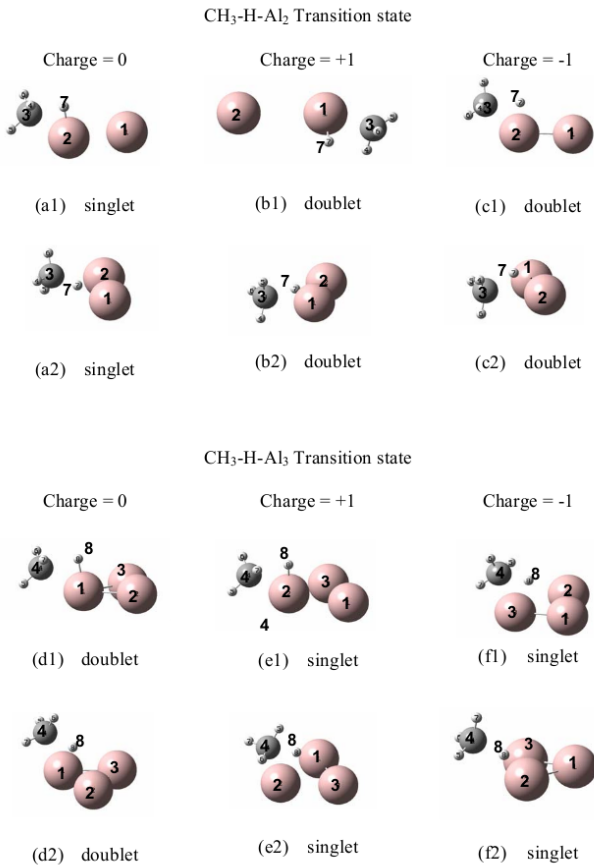


FIG. 6: (1) The lowest saddle point obtained by interpolation of the  $x$ - and  $y$ -values of Fig. 5 at the angle where the energy of Fig. 5 shows the lowest minimum. (2) The transition state obtained by the TSQN algorithm starting from the above saddle point, using as “reactants” and “products” the lowest lying structures of CH<sub>3</sub>-HAl<sub>*n*</sub><sup>*q*</sup> (cf. Fig. 3) and CH<sub>4</sub> + Al<sub>*n*</sub><sup>*q*</sup> (free)  $q = 0, 1, -1$ ,  $n = 3, 2$ . The exact atomic coordinates are mentioned in the text.

( $\text{\AA}$ , H-Al(2) = 1.90  $\text{\AA}$ ) with energies  $E = -485.1851 E_h$  and  $-485.0961 E_h$  respectively; therefore, the most stable structure is in the singlet state, by 0.408 eV lower than the separated Al<sub>2</sub><sup>+</sup> and H. By inserting CH<sub>3</sub>, the most stable structure between doublet [Fig. 3(b1)] and quartet [Fig. 3(b2)] is in doublet,  $E = -525.0911 E_h$ , by 0.29 eV (6.9 kcal/mol) lower than the separated Al<sub>2</sub><sup>+</sup> and CH<sub>4</sub>, where Al(2)-Al(1) = 3.73  $\text{\AA}$ , C(3)-Al(1) = 1.97  $\text{\AA}$ , C(3)-Al(1)-Al(2) = 113°, H(7)-Al(1) = 1.76  $\text{\AA}$ , H(7)-Al(1)-C(3) = 113°, dihedral angle H(7)-Al(1)-C(3)/Al(1)-C(3)-Al(2) = 0°.

We created energy contour diagrams similar to Fig. 4. The energies,  $y$ -, and  $x$ -values of the lowest lying saddle points from these diagrams are shown in Fig. 5 (b1,b2,b3) versus the angular position of each diagram’s plane. By interpolating the energy between the angles we see that the lowest saddle point occurs at the angle of 30° with  $x = 2.20 \text{\AA}$ ,  $y = -2.25 \text{\AA}$ ,  $E = -525.0167$

$E_h$ . Starting from this, [Fig. 6(b1)], and by relaxing all coordinates, we obtain by the TSQN algorithm [37] the lowest lying transition state (doublet) shown in Fig. 6(b2) with  $E = -525.0315 E_h$ , where Al(2)-Al(1) = 2.94  $\text{\AA}$ , C(3)-Al(1) = 2.25  $\text{\AA}$ , C(3)-Al(1)-Al(2) = 92°, H(7)-C(3) = 1.83  $\text{\AA}$ , H(7)-C(3)-Al(1) = 54°, dihedral angle H(7)-C(3)-Al(1)/C(3)-Al(1)-Al(2) = -1°. From these results, a dissociation barrier for the H-CH<sub>3</sub> bond breaking of 1.76 eV and a dissociation (desorption) barrier for the bond H-Al<sub>2</sub><sup>+</sup>CH<sub>3</sub> of 1.61 eV are derived.

The corresponding Mulliken atomic charges for the “reactants” CH<sub>4</sub> + Al<sub>2</sub><sup>+</sup>, “product” CH<sub>3</sub> + HAl<sub>2</sub><sup>+</sup>, and the transition state are given in Table II. We observe that, in the isolated systems, one electron is missing from the Al<sub>2</sub> cluster in all phases of the reaction. The three H atoms are not significantly affected, while in the process H(7) attracts some negative charge toward itself.

### C. Al<sub>2</sub><sup>-</sup> + CH<sub>4</sub>

The two lowest lying spin states of Al<sub>2</sub><sup>-</sup> at equilibrium are given in Table I. In agreement with Sun et al. (2006) [9], the ground state of Al<sub>2</sub><sup>-</sup> is  $4\Sigma_g^-$ , with bond length 2.58  $\text{\AA}$ , and 2.45  $\text{\AA}$  in the doublet state. The equilibrium structure of HAl<sub>2</sub><sup>-</sup> is given in Fig. 2(c1) (singlet,  $E = -485.4210 E_h$ ) and Fig. 2(c2) (triplet,  $E = -485.4402 E_h$ ), for both spin states isosceles triangle with angle 85° (singlet) and 90° (triplet), where the Al-Al bonds are comparable to the pure Al<sub>2</sub><sup>-</sup>. Therefore, the most stable structure is the triplet state 3 eV lower than the separated Al<sub>2</sub><sup>-</sup> and H. By inserting CH<sub>3</sub>, the most stable structure between doublet [Fig. 3(c1)] and quartet [Fig. 3(c2)] is the doublet state,  $E = -525.3689 E_h$ , by 0.01 eV lower than the separated Al<sub>2</sub><sup>-</sup> and CH<sub>4</sub>, where Al(2)-Al(1) = 2.53  $\text{\AA}$ , C(3)-Al(2) = 2.04  $\text{\AA}$ , C(3)-Al(2)-Al(1) = 152°, H(7)-Al(2) = 1.82  $\text{\AA}$ , H(7)-Al(2)-Al(1) = 48°, dihedral angle H(7)-Al(2)-Al(1)/Al(2)-Al(1)-C(3) = 3°.

The energies,  $y$ -, and  $x$ -values of the lowest lying saddle points from the corresponding energy contour diagrams, as in Fig. 4, are shown in Fig. 5 (c1,c2,c3) versus the angular position of each diagram’s plane. By interpolating the energy between the angles we see that the lowest saddle point occurs at the angle of 0° with  $x = 1.66 \text{\AA}$ ,  $y = 1.75 \text{\AA}$ ,  $E = -525.2833 E_h$ . Starting from this, [Fig. 6(c1)], and by relaxing all coordinates, we obtain by the TSQN algorithm [37] the lowest lying transition state (doublet) shown in Fig. 6(c2) with  $E = -525.2918 E_h$ , where Al(2)-Al(1) = 2.58  $\text{\AA}$ , C(3)-Al(2) = 2.72  $\text{\AA}$ , C(3)-Al(2)-Al(1) = 66°, H(7)-C(3) = 1.53  $\text{\AA}$ , H(7)-C(3)-Al(2) = 41°, dihedral angle H(7)-C(3)-Al(2)/C(3)-Al(2)-Al(1) = -48°. This results in a dissociation barrier for the H-CH<sub>3</sub> bond breaking of 1.44 eV and in a dissociation (desorption) barrier for the bond H-Al<sub>2</sub><sup>-</sup>CH<sub>3</sub> of 2.09 eV. The corresponding Mulliken atomic charges for the “reactants” CH<sub>4</sub> + Al<sub>2</sub><sup>-</sup>, “product” CH<sub>3</sub> + HAl<sub>2</sub><sup>-</sup>, and the transition state are given in Table II. We observe

that the extra electronic charge is distributed at the outermost parts of the molecule, for two reasons: Because  $\text{Al}_2$  remains negatively charged during the process, and because, as in the other cases,  $\text{H}(7)$  attracts some negative charge toward itself.

#### D. $\text{Al}_3 + \text{CH}_4$

The ground state of  $\text{Al}_3$  (doublet) is found to be equilateral triangle with a bond length of 2.54 Å. This is in good agreement with Sun *et al.* [9], Yang *et al.* [38], Hehre *et al.* [30], Ditchfield *et al.* [30], and the LSD approximation of Jones [39] who also finds an equilateral triangle with  $d = 2.46$  Å. There are nine valence electrons in  $\text{Al}_3$ . The molecular-energy levels from the first to the fourth are filled completely by eight electrons. The fifth level is the highest occupied level, which is partially filled with one electron [38]. The triplet is also an equilateral triangle with bond length 2.69 Å. The two lowest lying spin states of  $\text{Al}_3$  and  $\text{HAl}_3$  at equilibrium are given in Table I.

The equilibrium structure of  $\text{HAl}_3$  is given in Fig. 2(d1) (singlet,  $E = -727.83199 E_h$ ) and Fig. 2(d2) (triplet,  $E = -727.8269 E_h$ ), for both spin states a triangular pyramid with  $\text{Al-Al} = 2.59$  Å,  $\text{H-Al} = 1.91$  Å,  $\text{Al-H-Al} = 86^\circ$  in singlet, whereas in triplet it is slightly distorted. Therefore, the most stable structure is the sin-

glet state, 2.97 eV lower in energy than the separated  $\text{Al}_3$  and H.

By inserting  $\text{CH}_3$ , the most stable structure between doublet [Fig. 3(d1)] and quartet [Fig. 3(d2)] is in doublet,  $E = -767.7738 E_h$ , by 0.92 eV (21.3 kcal/mol) lower than the separated  $\text{Al}_3$  and  $\text{CH}_4$ , where  $\text{Al}(2)\text{-Al}(1) = 2.64$  Å,  $\text{Al}(3)\text{-Al}(2) = 2.54$  Å,  $\text{Al}(3)\text{-Al}(2)\text{-Al}(1) = 60^\circ$ ,  $\text{C}(4)\text{-Al}(1) = 1.98$  Å,  $\text{C}(4)\text{-Al}(1)\text{-Al}(3) = 149^\circ$ , dihedral angle  $\text{C}(4)\text{-Al}(1)\text{-Al}(3)/\text{Al}(1)\text{-Al}(3)\text{-Al}(2) = 143^\circ$ ,  $\text{H}(8)\text{-Al}(3) = 1.94$  Å,  $\text{H}(8)\text{-Al}(3)\text{-Al}(2) = 49^\circ$ , dihedral angle  $\text{H}(8)\text{-Al}(3)\text{-Al}(2)/\text{Al}(3)\text{-Al}(2)\text{-Al}(1) = 59^\circ$ .

From the corresponding energy diagrams, as in Fig. 4, we obtain the energies, y-, and x-values of the lowest lying saddle points as shown in Fig. 5 (d1,d2,d3) versus the angular position of each diagram's plane. By interpolating the energy between the angles we see that the lowest saddle point occurs at the angle of  $90^\circ$  with  $x = 1.80$  Å,  $y = 0.65$  Å,  $E = -767.6961 E_h$  [Fig. 6(d1)]. Starting from this, and by relaxing all coordinates, we obtain by the TSQN algorithm [37] the lowest lying transition state (doublet) shown in Fig. 6(d2) with  $E = -767.6891 E_h$ , where  $\text{Al}(2)\text{-Al}(1) = 2.81$  Å,  $\text{Al}(3)\text{-Al}(1) = 2.58$  Å,  $\text{Al}(3)\text{-Al}(1)\text{-Al}(2) = 57^\circ$ ,  $\text{C}(4)\text{-Al}(1) = 2.24$  Å,  $\text{C}(4)\text{-Al}(1)\text{-Al}(3)/\text{Al}(1)\text{-Al}(3)\text{-Al}(2) = 84^\circ$ ,  $\text{H}(8)\text{-C}(4) = 1.52$  Å,  $\text{H}(8)\text{-C}(4)\text{-Al}(1) = 50^\circ$ , dihedral angle  $\text{H}(8)\text{-C}(4)\text{-Al}(1)/\text{C}(4)\text{-Al}(1)\text{-Al}(3) = -25^\circ$ .

Atom	$(\text{CH}_4 + \text{Al}_2^q)$	Transition State	$\text{CH}_3\text{-HAl}_2^q$	$(\text{CH}_4 + \text{Al}_3^q)$	Transition State	$\text{CH}_3\text{-HAl}_3^q$
q=0						
Al(1)	-0.007	0.112	0.191	-0.007	0.127	0.299
Al(2)	-0.004	0.073	0.245	-0.001	-0.002	0.045
Al(3)	-0.471	-0.850	-0.573	-0.003	-0.002	0.041
C(4)	0.128	0.201	0.118	-0.475	-0.543	-0.574
H(5)	0.124	0.240	0.125	0.119	0.151	0.132
H(6)	0.126	0.240	0.118	0.118	0.142	0.128
H(7)	0.104	-0.017	-0.226	0.119	0.150	0.133
H(8)				0.129	-0.024	-0.206
q=+1						
Al(1)	0.445	0.475	0.626	0.294	0.374	0.412
Al(2)	0.445	0.598	0.700	0.251	0.292	0.426
C(3)	-0.500	-0.520	-0.569	0.321	0.374	0.426
H(4)	0.119	0.194	0.175	-0.507	-0.561	-0.584
H(5)	0.181	0.196	0.157	0.179	0.183	0.178
H(6)	0.165	0.192	0.157	0.185	0.194	0.180
H(7)	0.094	-0.137	-0.265	0.196	0.194	0.170
H(8)				0.078	-0.051	-0.196
q=-1						
Al(1)	-0.523	-0.397	-0.361	-0.330	-0.309	-0.234
Al(2)	-0.461	-0.363	-0.110	-0.327	-0.309	-0.269
Al(3)	-0.462	-0.529	-0.541	-0.338	-0.175	-0.007
C(4)	0.076	0.094	0.070	-0.480	-0.539	-0.545
H(5)	0.076	0.098	0.070	0.106	0.107	0.077
H(6)	0.114	0.118	0.071	0.099	0.114	0.092
H(7)	0.181	-0.020	-0.198	0.099	0.119	0.076
H(8)				0.172	-0.005	-0.189

TABLE II: The Mulliken atomic charges of the “reactants”  $\text{CH}_4 + \text{Al}_n^q$ , “products”  $\text{CH}_3 + \text{HAl}_n^q$ , and the corresponding transition states, at the lowest lying spin multiplicity (charge  $q = 0, 1, -1$ ), of all cases considered in this work,  $n = 2, 3$ .

Thus, in our approximation, the dissociation barrier for the H-CH<sub>3</sub> bond breaking is 1.55 eV and the dissociation barrier for the bond H-Al<sub>3</sub>CH<sub>3</sub> is 2.28 eV. Table II lists the corresponding Mulliken atomic charges for the “reactants” CH<sub>4</sub> + Al<sub>3</sub>, “product” CH<sub>3</sub> + HAl<sub>3</sub>, and the transition state. Similar trends are observed as in the Al<sub>2</sub> cases: During the process of the CH<sub>3</sub>Al<sub>3</sub>H hydride formation, H(8) attracts some negative charge toward itself, subtracting it mainly from the Al atom that binds CH<sub>3</sub>.

### E. Al<sub>3</sub><sup>+</sup> + CH<sub>4</sub>

Both lowest lying states of Al<sub>3</sub><sup>+</sup> in triplet (ground state) and singlet are found to be equilateral triangles with a bond length of 2.73 Å, E = -726.9895 E<sub>h</sub> and 2.57 Å, E = -726.9753 E<sub>h</sub> respectively. The two lowest lying spin states of Al<sub>3</sub><sup>+</sup> and HAl<sub>3</sub><sup>+</sup> at equilibrium are given in Table I.

The equilibrium structure of HAl<sub>3</sub><sup>+</sup> is given in Fig. 2(e1) (doublet, E = -727.8319 E<sub>h</sub>) and Fig. 2(e2) (quartet, E = -727.5511 E<sub>h</sub>), for both spin states a triangular pyramid with Al-Al = 2.67 Å, H-Al = 1.95 Å, Al-H-Al = 86° in doublet, whereas in quartet it is slightly distorted. Therefore, the most stable structure is the doublet state, 3.02 eV lower in energy than the separated Al<sub>3</sub><sup>+</sup> and H.

By inserting CH<sub>3</sub>, the most stable structure between singlet [Fig. 3(e1)] and triplet [Fig. 3(e2)] is in singlet, E = -767.5508 E<sub>h</sub>, by 0.46 eV (10.7 kcal/mol) lower than the separated Al<sub>2</sub><sup>+</sup> and CH<sub>4</sub>, where Al(2)-Al(1) = 2.76 Å, Al(3)-Al(1) = 2.48 Å, Al(3)-Al(1)-Al(2) = 63°, C(4)-Al(2) = 1.95 Å, C(4)-Al(2)-Al(1) = 152°, dihedral angle C(4)-Al(2)-Al(1)/Al(2)-Al(1)-Al(3) = -165°, H(8)-Al(1) = 1.85 Å, H(8)-Al(1)-Al(3) = 48°, dihedral angle H(8)-Al(1)-Al(3)/Al(1)-Al(3)-Al(2) = -76°.

Fig. 5 (e1,e2,e3) shows the energies, y-, and x-values of the lowest lying saddle points from the corresponding energy contour diagrams (as in Fig. 4), versus the angular position of each diagram’s plane. By interpolating the energy between the angles we see that the lowest saddle point occurs at the angle of 90° with x = 1.90 Å, y = 2.3 Å, E = -767.4569 E<sub>h</sub> [Fig. 6(e1)]. Starting from this, and by relaxing all coordinates, we obtain by the TSQN algorithm [37] the lowest lying transition state (singlet) shown in Fig. 6(e2) with E = -767.4672 E<sub>h</sub>, where Al(2)-Al(1) = 2.74 Å, Al(3)-Al(1) = 2.62 Å, Al(3)-Al(1)-Al(2) = 61°, C(4)-Al(2) = 2.19 Å, C(4)-Al(2)-Al(1) = 102°, dihedral angle C(4)-Al(2)-Al(1)/Al(2)-Al(1)-Al(3) = 96°, H(8)-C(4) = 1.53 Å, H(8)-C(4)-Al(2) = 52°, dihedral angle H(8)-C(4)-Al(2)/C(4)-Al(2)-Al(1) = -29°.

Thus, we find here a dissociation barrier for the H-CH<sub>3</sub> bond breaking of 1.06 eV and a dissociation (desorption) barrier for the bond H-Al<sub>3</sub><sup>+</sup>CH<sub>3</sub> of 2.25 eV. Analyzing the corresponding Mulliken atomic charges for the “reactants” CH<sub>4</sub> + Al<sub>3</sub><sup>+</sup>, “product” CH<sub>3</sub> + HAl<sub>3</sub><sup>+</sup>, and the

transition state given in Table II, we observe that the electronic charge is missing from the outer parts of the molecule. This is electrostatically reasonable. As in the other cases, the interacting H atom attracts some negative charge toward itself.

### F. Al<sub>3</sub><sup>-</sup> + CH<sub>4</sub>

In agreement with Sun *et al.* [9], and Ditchfield *et al.* [30] the optimized geometries of Al<sub>3</sub><sup>+</sup>, Al<sub>3</sub> and Al<sub>3</sub><sup>-</sup> are all equilateral triangles, in which Al<sub>3</sub> and Al<sub>3</sub><sup>-</sup> have almost equal bond lengths of 2.54 Å. In the ground state, (singlet) E = -727.2839 E<sub>h</sub> whereas in triplet E = -727.2679 E<sub>h</sub>. The two lowest lying spin states of Al<sub>3</sub><sup>-</sup> and HAl<sub>3</sub><sup>-</sup> at equilibrium are given in Table I.

The equilibrium structure of HAl<sub>3</sub><sup>-</sup> is given in Fig. 2(f1) (doublet), E = -727.8790 E<sub>h</sub>, where Al(2)-Al(1) = 2.74 Å, Al(3)-Al(2) = 2.52 Å, Al(3)-Al(2)-Al(1) = 63°, H(4)-Al(1) = 1.9 Å, H(4)-Al(1)-Al(3) = 49°, dihedral angle H(4)-Al(1)-Al(3)/Al(1)-Al(3)-Al(2) = 53° whereas in quartet [Fig. 2(f2)] E = -727.8702 E<sub>h</sub>. Therefore, the most stable structure is in doublet, by 2.58 eV lower than the separated Al<sub>3</sub><sup>-</sup> and H.

By inserting CH<sub>3</sub>, the most stable structure between singlet [Fig. 3(f1)] and triplet [Fig. 3(f2)] is in singlet, E = -767.8128 E<sub>h</sub>, by 0.32 eV (7.5 kcal/mol) lower than the separated Al<sub>2</sub><sup>-</sup> and CH<sub>4</sub>, where Al(2)-Al(1) = 2.64 Å, Al(3)-Al(1) = 2.43 Å, Al(3)-Al(1)-Al(2) = 71°, C(4)-Al(3) = 2.02 Å, C(4)-Al(3)-Al(1) = 162°, dihedral angle C(4)-Al(3)-Al(1)/Al(3)-Al(1)-Al(2) = -44°, H(8)-Al(3) = 1.89 Å, H(8)-Al(3)-Al(1) = 51°, dihedral angle H(8)-Al(3)-Al(1)/Al(3)-Al(1)-Al(2) = -52°.

From the corresponding energy contour diagrams, as in Fig. 4, the energies, y-, and x-values of the lowest lying saddle points versus the angular position of each diagram’s plane are shown in Fig. 5 (f1,f2,f3). By interpolating the energy between the angles we see that the lowest saddle point occurs at the angle of 120° with x = 1.73 Å, y = -1.75 Å, E = -767.7360 E<sub>h</sub> [Fig. 6(f1)]. Starting from this, and by relaxing all coordinates, we obtain by the TSQN algorithm [37] the lowest lying transition state (singlet) shown in Fig. 6(f2) with E = -767.7339 E<sub>h</sub>, where Al(2)-Al(1) = 2.57 Å, Al(3)-Al(1) = 2.54 Å, Al(3)-Al(1)-Al(2) = 70°, C(4)-Al(3) = 2.35 Å, C(4)-Al(3)-Al(1) = 123°, dihedral angle C(4)-Al(3)-Al(1)/Al(2)-Al(1)-Al(2) = -40°, H(8)-C(4) = 1.51 Å, H(8)-C(4)-Al(3) = 48°, dihedral angle H(8)-C(4)-Al(2)/C(4)-Al(2)-Al(1) = 2°.

Thus, in our approximation, the dissociation barrier for the H-CH<sub>3</sub> bond breaking 1.93 eV and the dissociation barrier for the bond H-Al<sub>3</sub><sup>-</sup>CH<sub>3</sub> is 2.12 eV. As far as the corresponding Mulliken atomic charges for the “reactants” CH<sub>4</sub> + Al<sub>3</sub><sup>-</sup>, “product” CH<sub>3</sub> + HAl<sub>3</sub><sup>-</sup>, and the transition state given in Table II are concerned, extra electronic charge is distributed in the three Al atoms and partially in the C atom, while the general trend still occurs: During the process, the interacting H atom at-



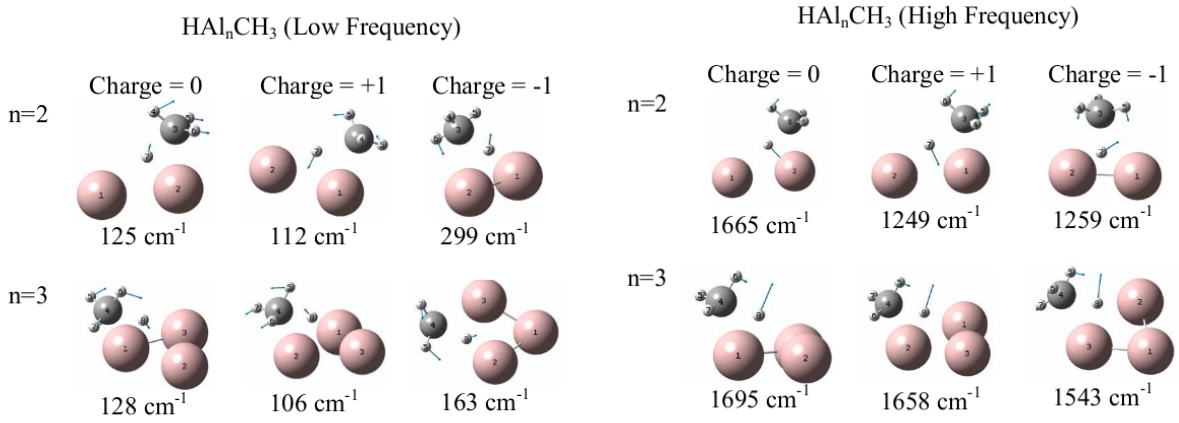


FIG. 7: Normal mode frequencies of the transmitted H atom at the transition state

tracts some negative charge toward itself. In all cases, the interacting H atom remains negatively charged by  $\sim 0.2$  electron.

## IV. RESULTS AND DISCUSSION

### A. Vibrational analysis

The Aluminum clusters considered,  $\text{Al}_2$  and  $\text{Al}_3$ , neutral as well as positively or negatively charged, can bind H rather strongly, either alone or in the presence of  $\text{CH}_3$ , where  $\text{CH}_3$  is bound to one Al atom, outside of the cluster, while H is bound to all Al atoms simultaneously, forming a triangle with  $\text{Al}_2$  (if positively charged, Al-H-Al are collinear) and a triangular pyramid with  $\text{Al}_3$ .

The main normal mode frequencies  $f = (1/2\pi)\sqrt{k/m^*}$  of the transmitted H are shown in Table III along with the corresponding force constant  $k$  and the effective mass  $m^*$ , which corresponds to the mass of one hydrogen atom in most cases (a little larger value indicates that the 3 H atoms are also slightly vibrating).

In the transition states (TSs), in all cases, the lowest frequency (55, 71, 47)  $\text{cm}^{-1}$  for  $\text{Al}_2\text{-H-CH}_3$ , charge= $(-1,0,1)$ , respectively, and (69, 65, 79)  $\text{cm}^{-1}$  for  $\text{Al}_3\text{-H-CH}_3$ , charge= $(-1,0,1)$ , respectively, corresponds essentially to a hindered rotation of  $\text{CH}_3$  around the transition position of the transmitted H atom, whereas the highest frequency (3180, 3147, 3211)  $\text{cm}^{-1}$  for  $\text{Al}_2\text{-H-CH}_3$  and (3137, 3140, 3141)  $\text{cm}^{-1}$  for  $\text{Al}_3\text{-H-CH}_3$ , respectively, corresponds essentially to the vibrations of the three H atoms of  $\text{CH}_3$  toward their central C atom. More interesting, however, are the normal modes next to the above, involving the vibrations of the transmitted H atom (cf. Fig. 7). The corresponding highest vibrational eigenfrequencies of the transmitted H atom (just below the above vibrations of the three H of  $\text{CH}_3$ ) are 1665  $\text{cm}^{-1}$  for  $\text{Al}_2\text{-H-CH}_3^{(q=0)}$ , 1021-1249  $\text{cm}^{-1}$  for  $\text{Al}_2\text{-H-CH}_3^+$ , 1047-1259  $\text{cm}^{-1}$  for  $\text{Al}_2\text{-H-CH}_3^-$ , also 1695  $\text{cm}^{-1}$  for  $\text{Al}_3\text{-H-}$

$\text{CH}_3^{(q=0)}$ , 1658  $\text{cm}^{-1}$  for  $\text{Al}_3\text{-H-CH}_3^+$ , and 931-1543  $\text{cm}^{-1}$  for  $\text{Al}_3\text{-H-CH}_3^-$ . On the other hand, the corresponding lowest vibrational eigenfrequencies of the transmitted H (just above the aforementioned hindered rotation of  $\text{CH}_3$ ) atom are 124  $\text{cm}^{-1}$  for  $\text{Al}_2\text{-H-CH}_3^{(q=0)}$ , 112  $\text{cm}^{-1}$  for  $\text{Al}_2\text{-H-CH}_3^+$ , 299  $\text{cm}^{-1}$  for  $\text{Al}_2\text{-H-CH}_3^-$ , and 128  $\text{cm}^{-1}$  for  $\text{Al}_3\text{-H-CH}_3^{(q=0)}$ , 1063  $\text{cm}^{-1}$  for  $\text{Al}_3\text{-H-CH}_3^+$ , and 163  $\text{cm}^{-1}$  for  $\text{Al}_3\text{-H-CH}_3^-$ . In the low frequency modes the transmitted H and  $\text{CH}_3$  move together, as if there were bonded, while in the highest of these frequencies the  $\text{CH}_3$  stays still with respect to the cluster whereas the transmitted H moves perpendicularly to the direction of the “bond” H- $\text{CH}_3$ .

description		$f$ ( $\text{cm}^{-1}$ )	$k$ ( $\mu\text{Dyn}/\text{\AA}$ )	$m^*$ (amu)
n=2, q=-1				
on C-Al-Al	H    Al-Al	947	549	1.0
on C-Al-Al	H $\perp$ Al-Al	1181	858	1.0
$\perp$ C-Al-Al		122	9	1.0
$\perp$ C-Al-Al		38	1.4	1.6
n=2, q=0				
on C-Al-Al	H    Al-Al	878	470	1.0
on C-Al-Al	H $\perp$ Al-Al	1177	852	1.0
$\perp$ C-Al-Al		133	11	1.0
n=2, q=+1				
on C-Al-Al	H    Al-Al	1395	1185	1.0
on C-Al-Al	H $\perp$ Al-Al	496	152	1.0
$\perp$ C-Al-Al		401	97	1.0
n=3, q=-1				
Al-Al-Al	H $\rightarrow$ $\text{CH}_3$	732	330	1.0
$\perp$ H- $\text{CH}_3$	H $\rightarrow$ middle of Al-Al	1044	662	1.0
$\perp$ H- $\text{CH}_3$	H $\rightarrow$ remote Al	636	284	1.2
n=3, q=0				
Al-Al-Al	H    C-Al-Al axis	665	292	1.1
Al-Al-Al	H $\perp$ C-Al-Al axis	573	203	1.0
$\perp$ Al-Al-Al		1118	759	1.0
n=3, q=+1				
Al-Al-Al	H $\rightarrow$ $\text{CH}_3$	440	130	1.1
$\perp$ Al-Al-Al		1242	936	1.0

TABLE III: Normal mode frequencies of the transmitted H at  $\text{CH}_3 - \text{HAl}_n^q$ . Frequency:  $f$ , Force constant:  $k$ , Effective mass ( $k/(2\pi f)^2$ ):  $m^*$

$\text{Al}_n$ / Charge	Adsorption barrier	Desorption barrier	Binding energy	Isolated cluster ( $\text{Al}_n$ )
	(eV / $\frac{\text{kcal}}{\text{mol}}$ )	(eV / $\frac{\text{kcal}}{\text{mol}}$ )	(eV / $\frac{\text{kcal}}{\text{mol}}$ )	Spin multiplicity
$\text{Al}_2$ / -1	1.45 / 33.4	2.09 / 48.2	-0.64 / -14.8	4
$\text{Al}_2$ / 0	1.00 / 23.1	2.04 / 47.02	-1.04 / -24.0	3
$\text{Al}_2$ / 1	1.78 / 41.0	1.62 / 37.4	0.16 / 3.7	2
$\text{Al}_3$ / -1	1.99 / 45.9	2.14 / 49.3	-0.15 / -3.5	1
$\text{Al}_3$ / 0	1.56 / 36.0	2.30 / 53.6	-0.74 / -17.1	2
$\text{Al}_3$ / 1	1.07 / 24.7	2.27 / 52.3	-1.20 / -27.7	3

TABLE IV: Adsorption barriers, desorption barriers, binding energies, for the reaction  $\text{CH}_4 + \text{Al}_n^q \rightleftharpoons \text{CH}_3 + \text{HAl}_n^q$ , along with the spin multiplicity of the isolated  $\text{Al}_n^q$  clusters.

In order to examine whether the dissociation is vibrationally enhanced [42, 43] we show in Table IV the calculated activation barriers and interaction energies, and in Table V the C-H distance at the transition state, along with the adsorption barrier height (compared to the corresponding energy of the free H- $\text{CH}_3$  molecule at the same C-H separation).

From Table IV we observe that in all cases except  $\text{Al}_2^{(q=+1)}$  the reaction  $\text{CH}_4 + \text{Al}_n^{(q)} \rightarrow \text{CH}_3 + \text{HAl}_n^{(q)}$  is exothermic, where the magnitude of the binding energy depends on the charge and on the total spin of the isolated cluster: In the exothermic cases it increases with increasing charge. Also, for  $n=3$  it increases with increasing isolated cluster spin, while for  $n=2$  it decreases. However, irrespective of the ground state of the isolated cluster, the reaction is favored with the lowest spin for the whole system (singlet or doublet). Note that the configuration of the Al cluster changes during the methane dissociation, since the transition state has a different geometry than the initial and the final state: After the transition H remains almost fixed, while  $\text{CH}_3$  moves toward one Al atom.

The last column of Table V shows the reduction of the bond energy (at the TS C-H separation) due to the

presence of the Al cluster. A negative sign means that the cluster unfavors the dissociation compared to the free  $\text{CH}_3$ . We observe that in most cases, except  $\text{Al}_3$  ( $q=0,-1$ ) the cluster favors the reaction. We shall see later that when this reduction is large, the transition rate constant takes on significant values at lower temperatures.

The free methane C-H bond length is 1.07 Å. We observe from Table V that in most cases the C-H separation at the transition state is  $\sim 1.5$  Å, whereas it is seen from the contour energy diagrams that the barrier is generally located rather in the curved region of the potential energy surface, indicating that it is not so “early” a barrier. Therefore, although we could not conclude that the dissociation is indeed vibrationally enhanced, the vibrational excitations could help to overcome the barrier.

As far as the dissociation pathway is concerned, one would say, at first glance, that in most cases H has to cover a rather short distance ( $\lesssim 0.5$  Å) to overcome the barrier. However, in all cases, as seen from the aforementioned frequencies, the potential well is deep enough to stabilize H in a methyl-aluminum-hydride.

n of $\text{Al}_n$	Charge	C-H distance at TS (Å)	Adsorption barrier (eV / $\frac{\text{kcal}}{\text{mol}}$ )	Energy of free $\text{CH}_3$ -H at the C-H distance of the TS	$\Delta E$ at the C-H distance of the TS
				(eV / $\frac{\text{kcal}}{\text{mol}}$ )	(eV / $\frac{\text{kcal}}{\text{mol}}$ )
2	-1	1.53	1.45 / 33.4	1.47 / 33.9	0.02 / 0.46
2	0	1.52	1.00 / 23.1	1.58 / 36.4	0.58 / 13.4
2	1	1.86	1.78 / 41.0	3.22 / 74.3	1.44 / 33.2
3	-1	1.50	1.99 / 45.9	1.40 / 32.3	-0.59 / -13.6
3	0	1.51	1.56 / 36.0	1.36 / 31.4	-0.20 / -4.6
3	1	1.52	1.07 / 24.7	1.58 / 36.4	0.51 / 11.8

TABLE V: The C-H distance at the transition state (TS), and the energy compared to the corresponding energy of the free H- $\text{CH}_3$  molecule at the same C-H separation.

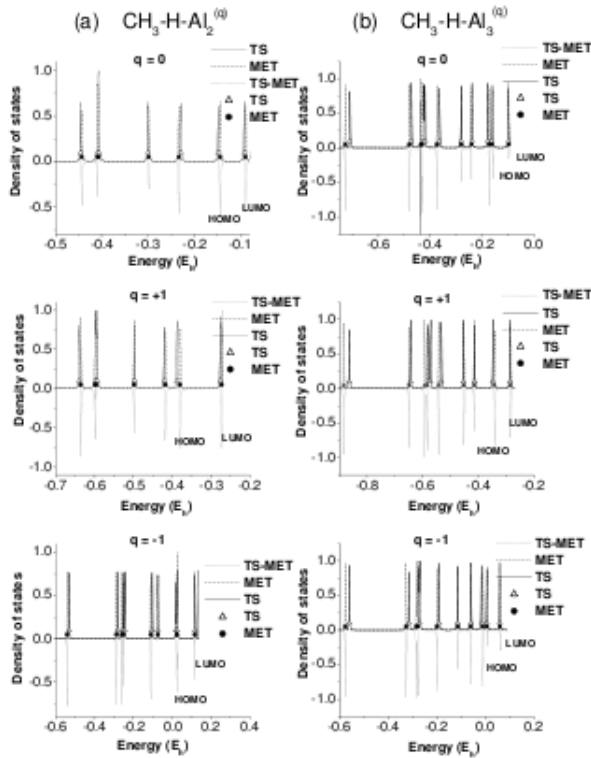


FIG. 8: Indicative density of states at the transition state (TS) (solid line) and at a nearby state (MET) (dashed line), defined by moving the H atom slightly toward  $\text{CH}_3$ , along with their difference (TS-MET), showing the trend toward higher or lower energy (dotted line). The points indicate the position of the computed one-electron levels. (a)  $\text{CH}_3+\text{HAl}_2$ , charge = 0,1,-1 and (b)  $\text{CH}_3+\text{HAl}_3$ , charge = 0,1,-1

### B. Orbitals involved in the transition

In order to examine the orbitals that are involved in the transition of H from  $\text{CH}_4+\text{Al}_n$  to  $\text{CH}_3+\text{HAl}_n$  we simulated a density of states  $\text{DOS}(E)=\frac{1}{2\pi}\text{Im}\left(\sum_j\frac{1}{E-E_j-i\delta}\right)$  both at the transition state (TS), and at a nearby state (“MET”), defined by moving the H atom slightly toward  $\text{CH}_3$ . Here  $E$  is the desired energy value and  $E_j$  are the computed one-electron levels with a small imaginary part,  $\delta=0.001$  a.u. The resulting DOS are shown in Fig. 8 ((a) for  $\text{CH}_3+\text{HAl}_2$  and (b) for  $\text{CH}_3+\text{HAl}_3$ ) for charge 0,1,-1 consecutively. We only report on those orbitals, which are affected by the H transition. As seen by the corresponding valence orbital electron densities (cf. Fig. 9), in all cases the orbital occupied by the transmitted H electron is bonding to the  $\text{Al}_n$  cluster and lies deeply below the HOMO, (the only even deeper orbital represents the formation of the three C-H bonds in  $\text{CH}_3$ ). If we refer the energies to the level of this bonding H- $\text{Al}_n$  orbital, (cf. Fig. 10) we observe that, in all cases, an antibonding C-H orbital lies higher by 8.16 eV (188.11 kcal/mol) [6.8

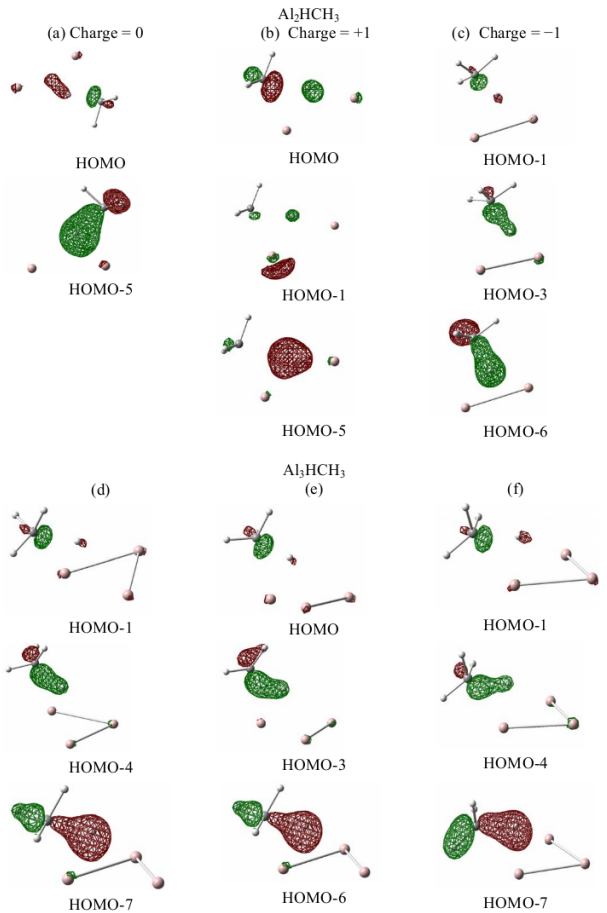


FIG. 9: The charge densities of the valence orbitals that are partially occupied by the electron of the transmitted H atom at the transition state. (a)  $\text{CH}_3\text{-H-Al}_2^{(q=0)}$  (b)  $\text{CH}_3\text{-H-Al}_2^{(q=+1)}$ , (c)  $\text{CH}_3\text{-H-Al}_2^{(q=-1)}$  (d)  $\text{CH}_3\text{-H-Al}_3^{(q=0)}$ , (e)  $\text{CH}_3\text{-H-Al}_3^{(q=+1)}$ , (f)  $\text{CH}_3\text{-H-Al}_3^{(q=-1)}$  The bonding and antibonding character is clearly displayed.

eV (156.81 kcal/mol) in  $\text{Al}_2^{(q=+1)}$ ], which in many cases is the HOMO or slightly lower than the HOMO, while in between, lying higher by  $\sim 2.72$  eV (62.72 kcal/mol) in  $\text{Al}_3$  and by  $\sim 5.44$  eV (125.44 kcal/mol) in  $\text{Al}_2$ , there is another C-H bonding orbital.

All other orbitals, lying in between, belong exclusively to either  $\text{CH}_3$  or  $\text{Al}_n$ , and are slightly affected in moving the H atom. We believe that the above low energies are responsible for the inactivity of  $\text{CH}_4$  near large Al clusters [10]. We note that the orbitals whose energies in Fig. 10 increase with increasing charge (just above and below the 0-level of the H- $\text{Al}_n$  bonding orbital) belong exclusively to  $\text{CH}_3$ , whereas those lying higher, whose energies in Fig. 10 in most cases decrease with increasing charge, belong to  $\text{Al}_n$ ; one of these forms the aforementioned H-C bonding orbital with C, which includes some electronic charge of the transmitted H.

For the H desorption, the transmitted H stays stably

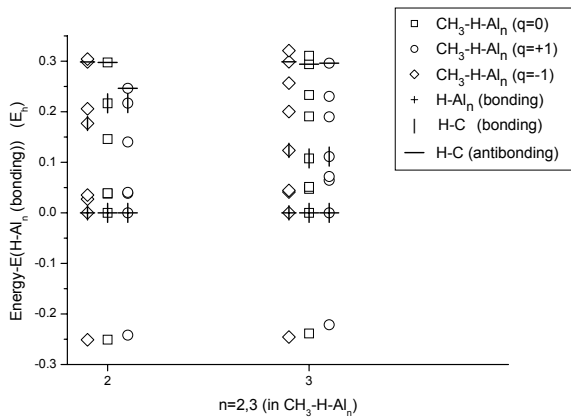


FIG. 10: The valence orbital energies at the transition states of  $\text{CH}_3\text{-H-Al}_n$  with respect to the deepest  $\text{H-Al}_n$  bonding orbital,  $n = 2, 3$ . The vertical axis is the energy in  $E_h$ . The horizontal axis is used to indicate the existence of the orbitals for each  $n$ : The orbitals of the neutral species ( $q = 0$ ) are displayed at the  $n$ -th level, while the orbitals of the charged species are displayed slightly to the right ( $q = +1$ ) and to the left ( $q = -1$ ) of the  $n$ -th level. Orbitals that are partially occupied by the electron of the transmitted H atom are indicated by dashes: “+” for the deepest  $\text{H-Al}_n$  bonding orbital, “—” for the highest  $\text{H-C}$  antibonding orbital, and “|” for the intermediate  $\text{H-C}$  bonding orbital.

at its potential well in all cases except for  $\text{Al}_2^+$  in going from the methyl-aluminum-hydride to the transition state, bonded with the outer  $\pi$  orbital of the cluster, while  $\text{CH}_3$  moves. As shown in Fig. 11, in all the cases except for  $\text{Al}_2^+$  some electronic charge of  $-0.2$  is transferred from H toward the Al cluster when  $\text{CH}_3$  moves from  $\text{HAl}_n\text{CH}_3$  to the transition state.

In case of  $\text{HAl}_2^+\text{CH}_3$  the H of the methyl-aluminum-hydride with electronic charge of  $-0.3$  moves away from the cluster by taking some electronic charge of  $0.2$  from the  $\text{CH}_3$  and leaving it to  $\text{Al}_2^+$ , thus staying as H with electronic charge of  $0.1$ . We note that this is the only endothermic reaction of all cases and the most favorable for the dissociation of  $\text{CH}_4$ . After the transition  $\text{CH}_4$  becomes neutral and the Al clusters remain at the corresponding spin polarization - not necessarily at the cluster ground state (the  $\text{Al}_3^-$  is in quartet).

### C. Spin distribution

Table VI (see also Fig. 12) shows the spin density (of the spin-polarized species) at the transition state, along with the distances from the C atom. We observe that in all cases the spin is distributed around the transmitted H atom which has the lowest spin polarization. The spin density is also increasing, beyond H, with increasing of the distance from the C atom, up to  $3.75 \text{ \AA}$  (remarkably there are many common distances from C in all species

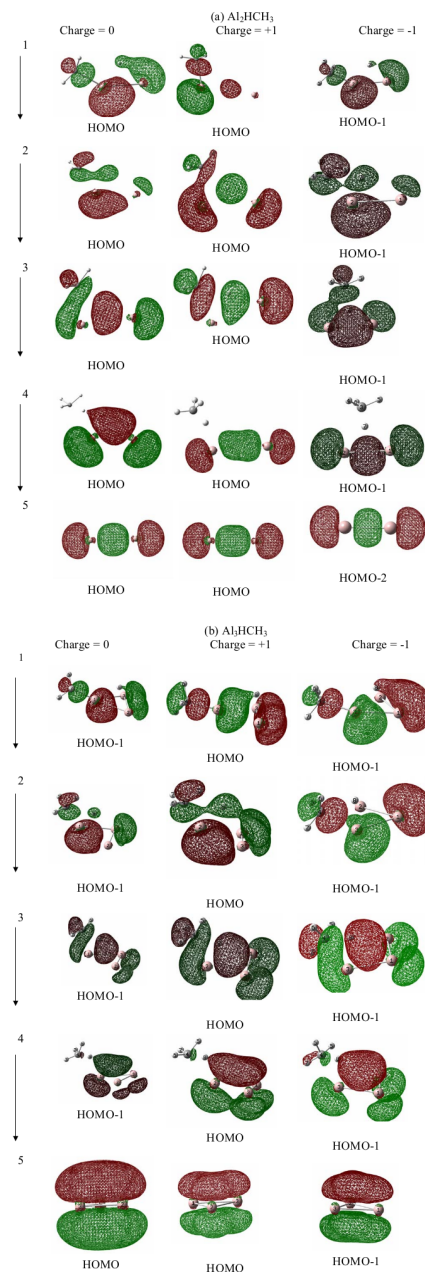


FIG. 11: The charge densities of the valence orbitals that are partially occupied by the electron of the transmitted H atom at the  $\text{CH}_3\text{Al}_n\text{H}$  hydride potential well (1), before the transition (2), at the transition state (3), after the transition (4) and at the  $\text{Al}_n$  cluster (5). (a)  $\text{Al}_2\text{HCH}_3^{(q=0,1,-1)}$ , (b)  $\text{Al}_3\text{HCH}_3^{(q=0,1,-1)}$ . The arrows on the left indicate a logical sequence in going through the aforementioned states 1-5.

considered), while in the larger systems ( $\text{Al}_3$ ) the spin density drops at larger distances.

	Al <sub>2</sub> q=0			Al <sub>2</sub> q=1			Al <sub>2</sub> q=-1		
Al(1)	2.25	3.73	1.069	1.91	2.28	0.096	1.91	2.90	0.526
Al(2)	1.76	2.38	0.621	1.91	3.78	0.389	1.86	2.71	0.500
C(3)	1.48	0	0.200	1.87	0	0.432	1.53	0	0.019
H(4)			-0.004			-0.000			-0.000
H(5)			0.004			0.009			0.001
H(6)			0.004			-0.016			0.001
H(7)	0	1.48	0.102	0	1.87	0.089	0	1.53	-0.010
Sum			2.000			1.000			1.000

	Al <sub>3</sub> q=0			Al <sub>3</sub> q=1			Al <sub>3</sub> q=-1		
Al(1)	1.72	2.24	0.065	2.5	3.83	0.701	2.9	4.29	0.695
Al(2)	2.47	3.78	0.516	1.74	2.19	0.204	2.1	3.30	0.882
Al(3)	2.62	3.97	0.398	2.5	3.83	0.701	1.76	2.34	0.447
C(4)	1.51	0	0.021	1.53	0	0.252	1.5	0	-0.016
H(5)			-0.000			-0.004			0.007
H(6)			-0.000			0.010			0.000
H(7)			0.002			0.010			0.000
H(8)	0	1.51	-0.003	0	1.53	0.124	0	1.50	-0.017
Sum			1.000			2.000			2.000

TABLE VI: Mulliken spin densities at the transition state (TS) of the spin-polarized species CH<sub>3</sub>-H-Al<sub>n</sub><sup>(q)</sup>, q = 0, 1, -1, n = 2, 3, (columns 3, 5, 7) along with the distances (in Å) from the C atom (column 2, 4, 6). The last H atom is the transmitted atom.

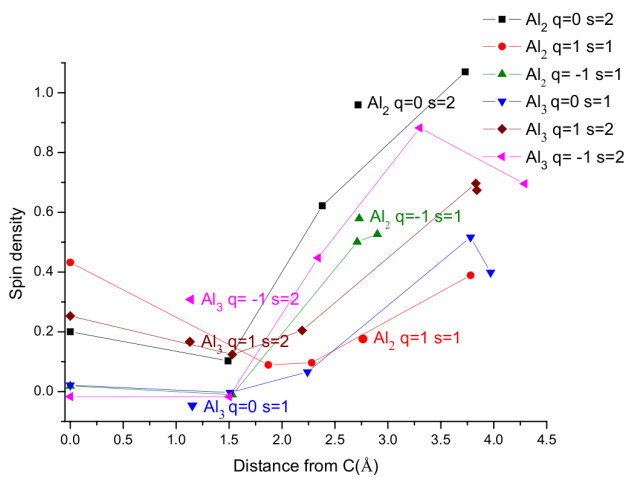


FIG. 12: The spin distribution at the transition state for all cases CH<sub>3</sub>+HAl<sub>n</sub><sup>q</sup>, at the lowest energy spin states; q is the charge = 0,1,-1 and s is the spin multiplicity.

#### D. Transition rate constants

Using the transition state theory (TST) in the harmonic approximation ( $\hbar\omega \ll k_B T$ ) [44] we computed the transition rate constant

$$k_{TST} = \frac{1}{2\pi} \frac{\prod_{i=0}^N \omega_i^{(0)}}{\prod_{i=1}^N \omega_i^{TS}} e^{-E_a/k_B T}$$

where  $\omega_i^{(0)}$  and  $\omega_i^{TS}$  are the vibrational frequencies in the stable well of CH<sub>3</sub>-H-Al<sub>n</sub> and the transition state, respectively, and  $E_a$  is the barrier height. The transition rate

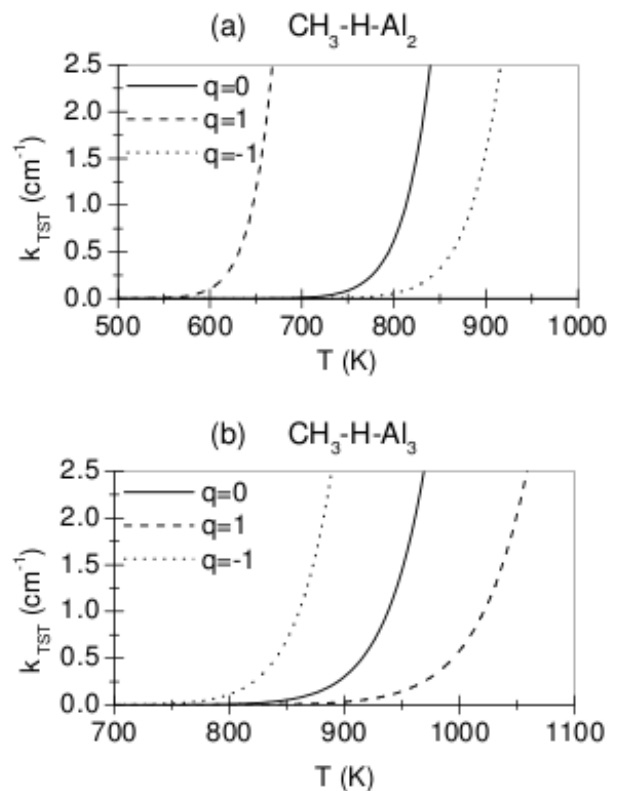


FIG. 13: The transition state theory rate constants  $k_{TST}$  in s<sup>-1</sup>, for the desorption of (a) CH<sub>3</sub>+HAl<sub>2</sub> and (b) CH<sub>3</sub>+HAl<sub>3</sub>, (charge = 0,1,-1)

constants (in s<sup>-1</sup>) for the recombinative CH<sub>4</sub> desorption are given in Fig. 13 as functions of the temperature. De-

pending on cluster size and the charge state, the recombinative  $\text{CH}_4$  desorption occurs at temperatures between  $\sim 400$  and  $700^\circ\text{C}$ . For  $n=3$  the temperature increases with increasing charge, while for  $n=2$  it decreases.

For the opposite reaction, the dissociative adsorption of  $\text{CH}_4$ , the  $\text{CH}_4$  molecule far from  $\text{Al}_n$  has still some imaginary frequencies. This is due to some spurious interaction between the fragments. However, these imaginary frequencies go to zero as  $\text{CH}_4$  is removed to infinity which means that the two separated parts can freely move and rotate about their centers. In this case, ordinary TST in the harmonic approximation is inapplicable so that no rate constant has been derived.

## V. CONCLUSIONS

Using density functional theory together with the B3LYP functional for exchange and correlation, we investigated the interaction of  $\text{CH}_4$  with small aluminum clusters of  $\text{Al}_n^{(q)}$   $n=2,3$  both neutral and charged, ( $q=-1,0,1$ ) and the formation of  $\text{CH}_3\text{-Al}_n\text{H}$  hydrides, in the lowest lying spin state. We summarize the general trends for the dissociation of methane on the small Al clusters found in this study.

Although  $\text{CH}_4$  does not interact with large Al clusters and bulk Al, it can interact with the small clusters investigated, with desorption temperatures of about  $\sim 400\text{-}700^\circ\text{C}$ . In all cases except  $\text{Al}_2^+$ , the reaction is exothermic. Generally H binds to positions with optimum charge densities, and when  $\text{CH}_3$  binds, H prefers to move further away from  $\text{CH}_3$ . Furthermore, in all cases, again except  $\text{Al}_2^+$ , the transmitted H, stays stably near the Al atoms, in going from the potential well of the  $\text{HAl}_n\text{CH}_3$  to the transition state, while only the  $\text{CH}_3$  moves.

In  $\text{HAl}_n\text{CH}_3$  hydride, the transmitted H atom attracts some electronic charge, which, in the transition state is

transferred to the Al atoms. Thus, it occupies mainly two orbitals, one antibonding H- $\text{CH}_3$  lying shallow (HOMO or HOMO-1), and one bonding H- $\text{Al}_n$  lying  $-8.16$  eV ( $188.16$  kcal/mol) deeper. The spin (if non-zero) is distributed around the transmitted H atom at moderate distances from the C atom (no more than  $\sim 3.5$  Å). The small Al clusters reduce the (free methane)  $\text{CH}_3\text{-H}$  dissociation barrier except for  $\text{Al}_3^{(q=-1,0)}$ . This is also reflected by the range of temperatures with significant transition rate constant  $k_{TST}$  for recombinative desorption. In all exothermic cases (i.e. except  $\text{Al}_2^+$ ) the binding energy increases with increasing charge ( $-1, 0, 1$ ). Thermal vibrations, generally, do not enhance the reaction. At the transition states, the lowest frequencies of about  $\sim 100$   $\text{cm}^{-1}$  correspond to small amplitude vibrations of  $\text{CH}_3$  (as a whole) around the transmitted H (the highest  $\sim 3000$   $\text{cm}^{-1}$  correspond to small amplitude vibrations of the three H atoms of  $\text{CH}_3$ ), while the transmitted H vibrates at high amplitude intermediate frequencies of  $\sim 1500$   $\text{cm}^{-1}$ , indicating the formation of rather stable methyl-aluminum-hydrides.

This study is continued with  $\text{Al}_4$  and  $\text{Al}_5$  clusters in order to make further decisions about the role of the local geometry on the interaction of non-d-electron small clusters with methane.

## Acknowledgments

Work supported by Action 8.3.1 Reinforcement Programme of Human Research Manpower - "PENED-2003" (Public expenditure by 90%), co-funded from the European Union by 75% and from the Hellenic State by 25% through the Operational Programme Competitiveness, 2000-2006. We would like to thank Dr. I. Petsalakis for useful discussions.

- 
- [1] O. Ingolfsson, H. Takeo, and S. Nonose, *J. Chem. Phys.*, **110**, 4382 (1999)
  - [2] M. D. Deshpande, D. G. Kanhere, I. Vasiliev, and R. M. Martin, *Phys. Rev. B.*, **68**, 035428 (2003)
  - [3] A. Groß, *J. Comput. Theor. Nanosci.*, **5**, 894 (2008)
  - [4] Z. P. Liu, and P. Hu, *J. Am. Chem. Soc.*, **125**, 1958 (2003)
  - [5] Ganbing Zhang, Shuhua Li, and Yuansheng Jiang, *Organometallics*, **22**, 3820 (2003)
  - [6] P. R. Kemper, J. Bushnell, M. T. Bowers, and G. I. Gelene, *J. Phys. Chem. A*, **102**, 8590 (1998)
  - [7] B. D. Leskiw, and A. W. Castleman, *Chem. Phys. Lett.*, **316**, 31 (2000)
  - [8] L. Hanley, S. A. Ruatta, and S. L. Anderson, *J. Chem. Phys.*, **87**, 260 (1987)
  - [9] J. Sun, W. C. Lu, H. Wang, Z.-S. Li, and C.-C. Sun, *J. Phys. Chem. A*, **110**, 2729 (2006)
  - [10] R. L. Hettich, *J. Am. Chem. Soc.*, **111**, 8582 (1989)
  - [11] H. Schwarz, *Int. J. Mass Spectrom.*, **237**, 75 (2004)
  - [12] C. Mosch, C. Koukounas, N. Bacalis, A. Metropoulos, A. Gross, and A. Mavridis, *J. Phys. Chem. C*, **112**, 6924 (2008)
  - [13] J. Behler, B. Delley, S. Lorenz, K. Reuter, and M. Scheffler, *Phys. Rev. Lett.*, **94**, 036104 (2005)
  - [14] J. Behler, B. Delley, K. Reuter, and M. Scheffler, *Phys. Rev. B*, **75**, 115409 (2007)
  - [15] C. Carbogno, J. Behler, A. Groß, and K. Reuter, *Phys. Rev. Lett.*, **101**, 096104 (2008)
  - [16] C. Carbogno, J. Behler, K. Reuter, and A. Groß, *Phys. Rev. B*, **81**, 035410 (2010)
  - [17] L. Österlund, I. Zorić, and B. Kasemo, *Phys. Rev. B*, **55**, 15452 (1997)
  - [18] R. Burgert et al., *Science*, **319**, 438 (2008)
  - [19] Taijin Zhou, Aimin Liu, Yirong Mo, and Hongbin Zhang, *J. Phys. Chem. A*, **104**, 4505 (2000)
  - [20] H. Öström, L. Triguero, M. Nyberg, H. Ogasawara,

- L. G. M. Pettersson, and A. Nilsson, *Phys. Rev. Lett.*, **91**, 046102 (2003)
- [21] J. Greeley and M. Mavrikakis, *J. Am. Chem. Soc.* **126**, 3910 (2004).
- [22] S. Sakong and A. Groß, *J. Catal.* **231**, 420 (2005).
- [23] S. Sakong and A. Groß, *J. Phys. Chem. A* **111**, 8814 (2007).
- [24] T. Mitsui, E. Hill, R. Curtis, and E. Ganz, *Phys. Rev. B*, **59**, 8123 (1999)
- [25] T. Nakajima, T. Tanaka, and K. Yamashita, *Surf. Sci.*, **444**, 99 (2000)
- [26] P. Hohenberg, and W. Kohn, *Phys. Rev.*, **136**, B864 (1964)
- [27] W. Kohn, and L. J. Sham, *Phys. Rev.*, **140**, A1133 (1965)
- [28] R. G. Parr, and W. Yang, *Density-functional theory of atoms and molecules* (Oxford Univ. Press, Oxford, 1989)
- [29] Gaussian 03, Revision D.01, M. J. Frisch, G. W. Trucks, H. B. Schlegel, G. E. Scuseria, M. A. Robb, J. R. Cheeseman, J. A. Montgomery, Jr., T. Vreven, K. N. Kudin, J. C. Burant, J. M. Millam, S. S. Iyengar, J. Tomasi, V. Barone, B. Mennucci, M. Cossi, G. Scalmani, N. Rega, G. A. Petersson, H. Nakatsuji, M. Hada, M. Ehara, K. Toyota, R. Fukuda, J. Hasegawa, M. Ishida, T. Nakajima, Y. Honda, O. Kitao, H. Nakai, M. Klene, X. Li, J. E. Knox, H. P. Hratchian, J. B. Cross, V. Bakken, C. Adamo, J. Jaramillo, R. Gomperts, R. E. Stratmann, O. Yazyev, A. J. Austin, R. Cammi, C. Pomelli, J. W. Ochterski, P. Y. Ayala, K. Morokuma, G. A. Voth, P. Salvador, J. J. Dannenberg, V. G. Zakrzewski, S. Dapprich, A. D. Daniels, M. C. Strain, O. Farkas, D. K. Malick, A. D. Rabuck, K. Raghavachari, J. B. Foresman, J. V. Ortiz, Q. Cui, A. G. Baboul, S. Clifford, J. Cioslowski, B. B. Stefanov, G. Liu, A. Liashenko, P. Piskorz, I. Komaromi, R. L. Martin, D. J. Fox, T. Keith, M. A. Al-Laham, C. Y. Peng, A. Nanayakkara, M. Challacombe, P. M. W. Gill, B. Johnson, W. Chen, M. W. Wong, C. Gonzalez, and J. A. Pople, Gaussian, Inc., Wallingford CT, 2004.
- [30] R. Ditchfield, W. J. Hehre, and J. A. Pople, *J. Chem. Phys.*, **54**, 724 (1971); W. J. Hehre, R. Ditchfield, and J. A. Pople, *J. Chem. Phys.*, **56**, 2257 (1972); P. C. Hariharan, and J. A. Pople, *Theo. Chim. Acta*, **28**, 213 (1973); P. C. Hariharan, and J. A. Pople, *Mol. Phys.*, **27**, 209 (1974); M. S. Gordon, *Chem. Phys. Lett.*, **76**, 163 (1980); M. M. Francl, W. J. Pietro, W. J. Hehre, J. S. Binkley, D. J. DeFrees, J. A. Pople, and M. S. Gordon, *J. Chem. Phys.*, **77**, 3654 (1982); G. A. Petersson, A. Bennett, T. G. Tensfeldt, M. A. Al-Laham, W. A. Shirley, and J. Mantzaris, *J. Chem. Phys.*, **89**, 2193 (1988); R. C. Binning Jr., and L. A. Curtiss, *J. Comp. Chem.*, **11**, 1206 (1990); G. A. Petersson, and M. A. Al-Laham, *J. Chem. Phys.*, **94**, 6081 (1991); J.-P. Blaudeau, M. P. McGrath, L. A. Curtiss, and L. Radom, *J. Chem. Phys.*, **107**, 5016 (1997); V. A. Rassolov, J. A. Pople, M. A. Ratner, and T. L. Windus, *J. Chem. Phys.*, **109**, 1223 (1998); V. A. Rassolov, M. A. Ratner, J. A. Pople, P. C. Redfern, and L. A. Curtiss, *J. Comp. Chem.*, **22**, 976 (2001)
- [31] A. D. Becke, *Phys. Rev. A*, **38**, 3098 (1988); C. Lee, W. Yang, and R. G. Parr, *Phys. Rev. B*, **37**, 785 (1988); B. Miehlich, A. Savin, H. Stoll, and H. Preuss, *Chem. Phys. Lett.*, **157**, 200 (1989); A. D. Becke, *J. Chem. Phys.*, **98**, 5648 (1993)
- [32] A. D. McLean, and G. S. Chandler, *J. Chem. Phys.*, **72**, 5639 (1980)
- [33] J. P. Perdew, K. Burke, and M. Ernzerhof, *Phys. Rev. Lett.*, **77**, 3865 (1996)
- [34] M. Head-Gordon, *J. Phys. Chem.*, **100**, 13213 (1996)
- [35] J. L. Whitten and H. Yang, *Surf. Sci. Rep.*, **24**, 55 (1996)
- [36] A. Groß, *Surf. Sci.*, **500**, 347 (2002)
- [37] C. Peng, P. Y. Ayala, H. B. Schlegel, and M. J. Frisch, *J. Comp. Chem.*, **17**, 49 (1996); C. Peng, and H. B. Schlegel, *Israel J. Chem.*, **33**, 449 (1994)
- [38] S. H. Yang, D. A. Drabold, J. B. Adams, and A. Sachdev, *Phys. Rev. B*, **47**, 1567 (1993)
- [39] R. O. Jones, *Phys. Rev. Lett.*, **67**, 224 - 227 (1991)
- [40] B. K. Rao, and P. Jena, *J. Chem. Phys.*, **111**, 1890 (1999)
- [41] C. -G. Zhan, F. Zheng, and D. A. Dixon, *J. Am. Chem. Soc.*, **124**, 14795 (2002)
- [42] J. C. Polanyi, and W. H. Wong, *J. Chem. Phys.*, **51**, 1439 (1969).
- [43] A. Groß and M. Scheffler, *Chem. Phys. Lett.*, **256**, 417 (1996)
- [44] P. Hänggi, P. Talkner, and M. Borkovec, *Rev. Mod. Phys.*, **62**, 251 (1990)